redin Revista Facultad de Ingeniería, Universidad de Antioquia, No.113, pp. 58-70, Oct-Dec 2024

Comparative CFD analysis of six VAWT turbines in the Chicamocha Canyon

Análisis comparativo en CFD de seis turbinas VAWT para el Cañón del Chicamocha

Juan Diego Rosero-Ariza[1*], **Jorge Luis Chacón-Velcasco**[1], **Germán González-Silva**[2]

[1]Escuela de Ingeniería Mecánica, Universidad Industrial de Santander. Campus Central, Carrera 27 Calle 9. Bucaramanga, Colombia
[2]Escuela de Ingeniería de Petróleos. Universidad Industrial de Santander. Campus Central, Carrera 27 Calle 9. Bucaramanga, Colombia

CITE THIS ARTICLE AS:

J. D. Rosero-Ariza, J. L. Chacón-Velasco and G. González-Silva. "Comparative CFD analysis of six VAWT turbines in the Chicamocha Canyon", *Revista Facultad de Ingeniería Universidad de Antioquia*, no. 113, pp. 58-70, Oct-Dec 2024. [Online]. Available: https://www.doi.org/10.17533/udea.redin.20240413

ARTICLE INFO:

Received: November 01, 2023
Accepted: April 25, 2024
Available online: April 25, 2024

KEYWORDS:

Fluid dynamics; aerodynamic; wind energy

Dinámica de fluidos; aerodinámica; energía eólica

ABSTRACT: Micro wind power generation through vertical axis wind turbines for low wind velocity in the department of Santander, Colombia, is viable due to the physical characteristics of the region. However, there are crucial factors for the development of a turbine for the region such as turbine typology, robustness, aspect ratios, etc. For this reason, it is a good practice to perform simulations through computational fluid dynamics (CFD) to predict the performance of the turbine in operation. In this context, an analysis of six configurations of a Darrieus-type VAWT turbine with the asymmetric profile DU06W200 and straight blades, which were obtained by an algorithm considering the factors mentioned above was carried out. The height-diameter ratios to be analyzed were 0.25 (with chord lengths of 0.117 and 0.173 m), 0.4 (with chord lengths of 0.0929 and 0.137 m) and 1 (with chord lengths of 0.0587 and 0.0864 m). It can be concluded that with a ratio of 0.25 and a rope length of 0.173 m, it is possible to obtain an average Power Coefficient of 0.31, which is an outstanding value due to the low wind velocity of the region of interest.

RESUMEN: La micro generación de energía eólica a través de turbinas eólicas de eje vertical para bajas velocidades de viento en el departamento de Santander, Colombia es viable, debido a las características físicas de la región. Sin embargo, existen factores cruciales para el desarrollo de una turbina para la región como la tipología de la turbina, solidez, relaciones de aspecto, etc. Por tal motivo, es una buena práctica realizar simulaciones por medio de la dinámica de fluidos computacional (CFD) con el fin de predecir el desempeño que tendrá la turbina en operación. Es por esto, que se realizó un análisis de seis configuraciones de una turbina VAWT tipo Darrieus de álabes rectos utilizando el perfil asimétrico DU06W200 las cuales fueron obtenidas por un algoritmo que tiene en cuenta los factores mencionados con anterioridad. Las relaciones de altura-diámetro a analizar fueron 0,25 (con longitudes de cuerda de 0,117 y 0,173 m), 0,4 (con longitudes de cuerda de 0,0929 y 0,137 m) y 1 (con longitudes de cuerda de 0,0587 y 0,0864 m). Se puede concluir con la relación de 0,25 y una longitud de cuerda de 0,173 m es posible obtener un Coeficiente de Potencia promedio de 0,31 siendo este un valor sobresaliente debido a la baja velocidad de viento de la región de interés.

1. Introduction

One of the 7 Sustainable Development Goals proposed by [1] is Ensuring access to affordable, secure, sustainable and modern energy. Progress on this goal has been positive in Colombia as energy becomes more sustainable

* Corresponding author: Juan Diego Rosero-Ariza
E-mail: juandiegorosero.120@gmail.com
ISSN 0120-6230
e-ISSN 2422-2844

In previous investigations, the feasibility of wind power generation in the Chicamocha Canyon was verified by determining the average annual wind power, which is 485 $[W/m^2]$. In addition, building the wind turbine blades using the aerodynamic profile DU06W200 is 14% more efficient than the commercially used NACA0018; this is an asymmetrical profile. [2] It is necessary a generator to produce electrical energy from the wind; this generator converts the kinetic energy of the wind into electrical energy through a wind turbine system. [3]

DOI: 10.17533/udea.redin.20240413

- **Nomenclature**
  - VAWT= Vertical axis wind turbine
  - HAWT= Horizontal axis wind turbine
  - W= Local velocity on the airfoil
  - $Re_c =$ Reynolds number based on chord
  - $C_l =$ Lift Coefficient
  - N= Number of blades
  - $C_d =$ Drag Coefficient
  - $u_i =$ Velocity Vector
  - $\sigma =$ Turbine solidity
  - $x_i =$ Position vector
  - Cp= Power Coefficient
  - t= Time
  - λ ó TSR= Tip speed ratio
  - $t_{ji} =$ Viscous stress tensor
  - A= Rotor Swept Area
  - P= Pressure
  - H= Rotor height
  - $\mu =$ Molecular viscosity
  - D= Rotor diameter
  - $s_{ij} =$ Strain rate tensor
  - R= Rotor radius
  - IT= Turbulent Intensity
  - c= Chord lenght
  - LS= Length Scale
  - Pt= Total Energy
  - $\beta =$ Turbulence modeling constant
  - Pd= Desired power
  - $\sigma_k y \sigma_\omega =$ Turbulent Schmidt numbers
  - $\rho =$ Air density
  - $\gamma =$ Mixed model coefficient
  - V= Velocity
  - $v_t =$ Turbulent diffusivity
  - $\theta =$ Turning angle in the cycle
  - $F_1 =$ Function coefficient
  - $\alpha =$ Attack angle
  - $v =$ Turbulent viscosity
  - T= Torque
  - $k =$ Turbulence kinetic energy.
  - $\omega =$ Angular Velocity
  - $\varepsilon =$ Energy dissipation rate.
  - $C_t =$ Radial force coefficient

The optimal value of the solidity of the turbine (σ), according to [4], is between 0.3 and 0.4 because the maximum value of the Power Coefficient *(Cp)* is there, which allows knowing the performance of the turbine.

A Cp of 0.5996 with a σ of 0.3 was proposed by [5]. However, the dimensions of the latter are considerably large for the installation of VAWT turbines in the region of interest. On the other hand, [6] suggests a design with a solidity (σ) of 1.2, obtaining a Cp 2.3 times lower than the design proposed by the first author. Despite this, the proposed design obtained good results at low velocities $(3m/s)$, this being the critical velocity as it is the lowest recorded according to [2] in the study region.

Based on the above, a parametric optimization of a Darrieus-type VAWT turbine will be performed considering the asymmetric profile DU06W200 using Computational Fluid Dynamics (CFD) in 2D, since it is an affordable and practical approach to simulate the flow field around a VAWT compared to experiments that incur higher costs, especially in the design optimization process. [7]. In this analysis, six possible configurations were considered and, were developed using an algorithm. As input data, there are physical variables of the region, and as output, the height-diameter and chord length configurations are obtained. As a result, it was obtained that one of the configurations has an average Power Coefficient of 0.31, reaching a maximum value of 0.42, which demonstrates the optimal behavior of the developed configuration.

2. Methodology

Figure 1 shows the scheme applied in the present study. The work is composed of two components: firstly, the design of an algorithm for the configurations of the turbines, and secondly, the CFD analysis of six VAWT turbine configurations for a critical wind velocity of $4.5m/s$ and a maximum velocity of $7m/s$, which were taken from the literature in a previous analysis.

The methodology employed in this study is illustrated in Figure 1. The research comprises two primary components. Firstly, an algorithm was designed to optimize turbine configurations. Secondly, Computational Fluid Dynamics (CFD) analysis was conducted for six Vertical Axis Wind Turbine (VAWT) configurations, considering a critical wind velocity of $4.5m/s$ and a maximum velocity of $7m/s$. These configurations were sourced from the literature through a prior analysis.

2.1 Algorithm design

The algorithm considers various input variables, encompassing both the physical parameters of the region, such as wind density (ρ) and wind velocity (V), as well as turbine-specific variables including the number of blades (N), desired power (Pd), and angle of attack (α). The algorithm generates output variables related to turbine dimensions, including radius (R), height (H), two possible chord length (c), and consequently, two potential values for turbine solidity (σ). The algorithm was structured with a predefined set of constraints, informed by an extensive literature review. These constraints encompass both upper and lower bounds for each variable, grounded in the physical characteristics of the Chicamocha Canyon. A

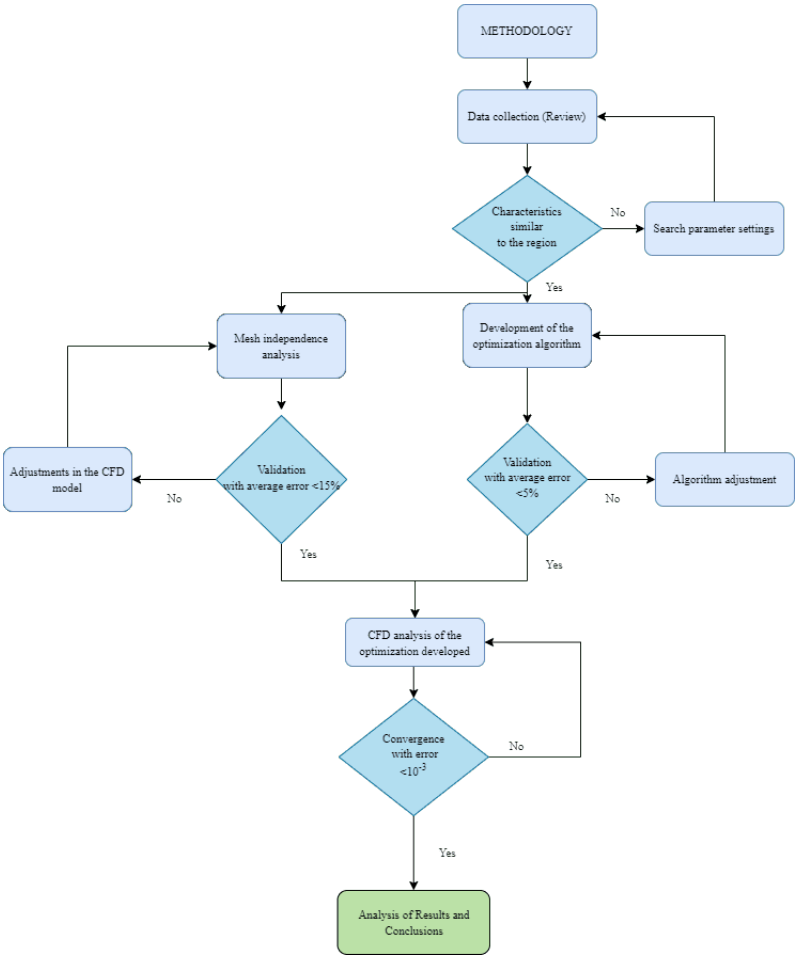

Figure 1 Methodology employed in the investigation. Author

Table 1 Algorithm Restriction [8]

Algorithm restrictions	
Variable	**Operation Rate**
AD	[0.25-2]
Cp máx	0.5926 (Betz's Limit)
σ	[0.2-0.5]
Tip Speed Ratio (λ)	[4–6]

comprehensive overview of these restrictions is presented in Table 1. For a visual representation of the algorithms flow, refer to Figure 2.

The efficiency of a vertical axis wind turbine (VAWT) is fundamentally associated with the Tip Speed Ratio (TSR or λ), which is the result of linear velocity on the tip of the rotor divided by the wind-free stream velocity [9], a function of angular velocity (ω), undisturbed wind velocity (V), and rotor radius (R), as established by [10] and [11]. The other parameter is the solidity (σ), which is related to the number of blades (N), chord length (c), and rotor radius. Equation 3 illustrates the relationship concerning TSR, while Equation 2 defines the relationship regarding solidity; these parameters are pivotal in evaluating and optimizing the performance of the VAWT configurations under investigation:

$$\lambda = \frac{\omega R}{V} \tag{1}$$

$$\sigma = \frac{Nc}{R} \tag{2}$$

The Reynolds number of the blades can be seen in equation Equation 3, where *c* is the chord length, *v* is the kinematic air velocity and *w* is the relative air velocity with respect to the airfoil.

$$Re_c = \frac{cw}{v} \tag{3}$$

The turbine's efficiency is expressed through the Power Coefficient *(Cp)*, which quantifies the proportion of energy generated by the turbine in relation to the total wind energy passing through the area it sweeps, as detailed in [12, 13]. This coefficient is essential for assessing the performance of the wind turbine in the research area of the current

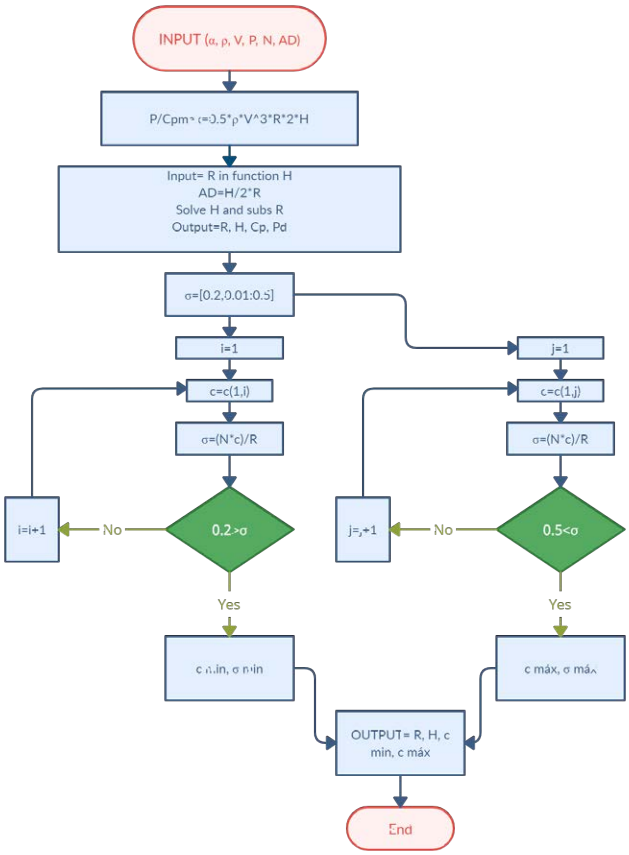

Figure 2 Algorithm flowchart. [8]

investigation and is defined by Equation 4, as described in the work of [14, 15]. In this equation, *PT* represents the total energy, ρ denotes air density, *V* is the wind velocity, and *A* is the swept area of the turbine.

$$C_p = \frac{P_T}{P_{\text{wind}}} = \frac{P_T}{\frac{1}{2}\rho V^3 A} \tag{4}$$

$$P_T = \omega * T_{fa} \tag{5}$$

$$T_{fa} = \frac{1}{2\pi}\int_0^{2\pi} T d\theta \tag{6}$$

In this equation, θ represents the angle in the cycle, α denotes the angle of attack, and *T* is expressed according to Equation 7, as described in [16]. In this reference, C_t it represents the radial force coefficient, as defined in Equation 8, while *W* is the local velocity at the aerodynamic profile, as explained in Equation 9.

$$T = \frac{1}{2} C_t \rho A R W^2 \tag{7}$$

$$C_t = C_l \sin\alpha - C_d \cos\alpha \tag{8}$$

$$W = \sqrt{(R\omega + V\cos\theta)^2 + (V\sin\theta)^2} \tag{9}$$

2.2 Computational Fluid Dynamics (CFD)

It consists of using computers and numerical techniques to solve all those physical problems related to the movement of fluids. Considering that the use of the tool substantially reduces time and costs in new designs as well as having a high level of detail, facilitating parametric studies, and obtaining a large amount of information without the additional cost of sensors [17].

The 2D models that do not consider the 3D effects like tip vortex, furthermore, this models using the URANS (Unsteady Reynolds Averaged Navier Stokes) transition model has obtained good results in the mechanical power and Power Coefficient with an overestimation of 6-8%. [18]

Incorporating Computational Fluid Dynamics (CFD) analysis, the primary objective is to solve the conservation equations for mass and momentum, elucidated in [19].

The expressions for these conservation equations are represented by Equations 10 and 11, respectively:

$$\frac{\partial u_i}{\partial x_i} = 0 \tag{10}$$

$$\rho\frac{\partial u_i}{\partial t} + \rho u_j \frac{\partial u_i}{\partial x_i} = -\frac{\partial p}{\partial x_i} + \frac{\partial t_{ji}}{\partial x_j} \tag{11}$$

The vectors u_i and xrepresent velocity and position, t denotes time, p stands for pressure, ρ represents density, and t_{ji} is the viscous stress tensor defined by Equation 12.

$$t_{ji} = 2\mu s_{ij} \tag{12}$$

Where μ is the molecular viscosity, and s_{ij} is the strain rate tensor expressed in Equation 13.

$$s_{ij} = \frac{1}{2}\left(\frac{\partial u_i}{\partial x_j} + \frac{\partial u_j}{\partial x_i}\right) \tag{13}$$

Turbulence models play a critical role in ensuring the quality and accuracy of the numerical solution, particularly concerning angles of attack and lift loss in the airfoil, as emphasized in [20]. Due to computational constraints associated with Large Eddy Simulation (LES) or Direct Numerical Simulation (DNS) approaches, researchers predominantly focus on Reynolds-Averaged Navier-Stokes (RANS) models.

As detailed in [21], the $k-\omega$ Shear-Stress Transport (k- ω-SST) turbulence model demonstrates superior performance in terms of stability, reliability, and agreement with experimental data compared to the traditional $k-\omega$ models. This model is especially advantageous in predicting turbulent boundary layers up to separation and analyzing compressible flows and separation flows under adverse pressure gradients, both of which are significant phenomena in real Darrieus turbine operation, as corroborated by [21]. Consequently, the $k-\omega$-SST approach stands out as a highly preferable solution for simulating and understanding the behavior of turbulent flows in the context of Darrieus turbine operation.

According to multiple sources [7, 19, 20, 22], the kω-SST turbulence stands out as the optimal choice for conducting Computational Fluid Dynamics (CFD) simulations specifically tailored for Darrieus turbines. Its superiority is attributed to its ability to effectively handle boundary layer separation and free shear flows, which are critical aspects prevalent in the aerodynamics of Darrieus turbines.

The $k-\omega$-SST turbulence model operates on empirical foundations, relying on model transport equations for turbulence kinetic energy (k) and the specific dissipation rate (ω) [23]. As a two-equation Reynolds Averaged Navier-Stokes (RANS) model, it integrates key features from both the $\mathrm{k}-\omega$ model formulation for free stream flow and $\mathrm{k}-\omega$ formulations. This unique characteristic is based on a transport equation for turbulent kinetic energy tailored to the rotor boundary layer [24].

Table 2 Geometric dimension [8]

Geometric dimensio	
Variable	**Dimension**
L	30R
L1	10R
L2	20R
H	10R
D-R	2.4R

In the study conducted by [25], the resulting equations for k and ω are as follows, demonstrated in Equations 14 and 15, respectively.

$$\rho\frac{Dk}{Dt} = \tau_{ij}\frac{\partial \bar{u}_i}{\partial x_j} - \beta * k\rho\omega + \frac{\partial}{\partial x_j}\left[\left(\mu + \frac{\mu_T}{\sigma_k}\right)\frac{\partial k}{\partial x_j}\right] \tag{14}$$

$$\rho\frac{D\omega}{Dt} = \frac{\gamma}{v_t}\tau_{ij}\frac{\partial \bar{u}_i}{\partial x_j} - \beta * \rho\omega^2 + \frac{\partial}{\partial x_j}\left[\left(\mu + \frac{\mu_T}{\sigma_\omega}\right)\frac{\partial \omega}{\partial x_j}\right] + 2\rho\left(1 - F_1\right)\sigma_\omega\frac{1}{\omega}\frac{\partial k}{\partial x_j}\frac{\partial \omega}{\partial x_j} \tag{15}$$

where $\beta*$ is a turbulence modeling constant, σ_k and σ_ω are turbulent Schmidt numbers, γ is a blended model coefficient, v_t is the turbulent diffusivity and F_1 is a function coefficient.

2.3 Boundary conditions

According to [21], the geometry of the turbines is used with a non-slip condition, which makes it possible to maintain zero velocity realistically on the surface of the turbine. The computational domain recommended by [19] for VAWT turbines is at least 60D wide, 40D upstream of the rotor, and 100D downstream of the rotor, where D is the diameter of the VAWT rotor; however, [25] concluded that a better result is obtained with a computational domain of 60D wide, 60D upstream of the rotor and 143D downstream of the rotor. The dimensions of the actual model, properties of the fluid, solutions methods and model configurations are determined by Tables 2 and 3.

The rotors were placed in a rotating region within a larger rectangular domain with top and bottom "symmetry", a velocity input, and a zero-gauge pressure output. A more refined mesh was created over the rotating region, and a sliding condition was applied to the walls to avoid locking effects. Verified by data from the Chicamocha Canyon, Santander, Colombia, the maximum and minimum entry

Table 3 Fluid properties and configuration. Author

Fluid: air	
Property	**Value**
Density	$1.225kg/m^3$
Viscosity	$1.7894^e - 5kg/m^*s$
Velocity	$4.5m/s - 7m/s$
Pressure	0 Pa
Temperature	300K
Parameter	**Value**
Pressure-Velocity Coupling	SIMPLE
Gradient	*Least Squares Cell-Based*
Pressure	*Second Order*
Moment	*Second Order Upwind*
Turbulent kinetic energy	*Second Order Upwind*
Specific dissipation rate	*Second Order Upwind*
Transitional formulation	*Second Order Implicit*
Solver	*Pressure Based*
Velocity	*formulation Absolute*
Time	*Transient*
Space	*2D space planar*

velocities were 7 and 4.5 m/s respectively, with a turbulence intensity of 4.11%. The angular velocities, ω, were varied in order to achieve an optimal λ according to [4, 23] is between 4 and 6. Six different designs were analyzed and evaluated. Three variables were investigated: the length of the chord (c), the radius of the turbine (R), and the height of the turbine (H). The information can be seen in Figure 3.

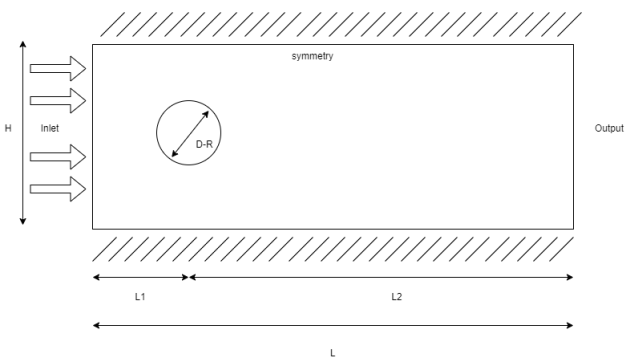

Figure 3 Geometric Model. Author

3. Discussion and analysis of results

3.1 Algorithm results

Firstly, an algorithm was developed in the MATLAB R2021a software, in which the radius, chord length and blade height of a straight-bladed Darrieus turbine for low wind velocity $(4.5m/s)$ are obtained, this being the critical velocity in the Chicamocha Canyon region.

Table 4 Fluid properties and configuration. Author

Algorithm validation			
Variable	**Value by [4]**	**Algorithm value**	**% Error**
R (m)	3	3	0%
H (m)	5	4.99	0.2%
c1 (m)	0.333	0.204	38.74%
c2 (m)	0.333	0.333	0%
$\sigma 1$	0.333	0.204	38.74%
$\sigma 2$	0.333	0.333	0

Table 5 Algorithm results [8]

Algorithm results				
Inlet				
$\rho\ (\mathrm{kg/m^3})$	V (m/s)	N	Pd (W)	$Cp_{\max}$
1.225	4.5	3	100	0.5996
Output				
AD	R (m)	H (m)	c_1 (m)	c_2 (m)
0.25	1.73	0.864	0.117	0.173
0.4	1.37	1.09	0.0929	0.137
1	0.864	1.73	0.0587	0.0864

The algorithm was validated with the reference [5] introducing physical variables $(\rho = 1.225\,\mathrm{kg/m3}, P = 1\,\mathrm{kW}, \mathrm{V} = 4.5\,\mathrm{m/s}), \mathrm{Cpmax} = 0.5996, \mathrm{N} = 3)$, the results and errors can be seen in table 4.

As shown in Table 4, the algorithm presents an almost zero error (0.2%) as the maximum in the turbine height. The present algorithm presents an improvement because it allows analyzing two different chord lengths for the same height-diameter relationship. Six different configurations were obtained as shown in Table 5, which will be validated and compared later in the CFD analysis.

3.2 Mesh independence and quality

A comparative study of three different grids was conducted, in which Cp was analyzed in each of them and compared with experimental data from [18]. In the comparison, the number of elements in the meshes began with 218,647 elements, and then the Intensity (IT) and Length Scale (LS) parameters were refined or adjusted. The characteristics of this mesh are detailed in Table 6, while the quality parameters are presented in Tables 7 and 8. In Figure 6, in part a.), it can be seen the general velocity contours presented, where it is observed that each blade leaves a wake with a velocity of around $3.44m/s$, which directly influences the attack of the next blade Additionally, the highest velocity appears at the leading edge of each profile as seen in part b.)

According to [24], the principal mesh quality parameters are aspect ratio, skewness, and orthogonal quality. A high aspect ratio value can affect cell symmetry, potentially

Table 6 Quality mesh 2 and 3. Author

Principal parameters of the meshes				
Mesh	**IT& LS**	**Total Elements**	**y+**	**Elements in rotate**
Mesh 1	IT=5% LS=1	218647	0.85	139826
Mesh 2	IT=4.11% LS=1	889968	0.76	750142
Mesh 3	IT=4.11% LS=0.007	889968	0.76	750142

Table 7 Quality mesh 2 and 3. Author

Quality mesh 2 and 3				
Parameter	**Minimum Value**	**Maximum Value**	**Average Value**	**Optimal Value**
Aspect Ratio	3.0012	54.821	3.300	To avoid significant changes in general
Skewness	5.07e-7	0.9032	6.51e-2	<0.95
Orthogonal quality	7.68e-2	0.9	0.84	Values close to 1

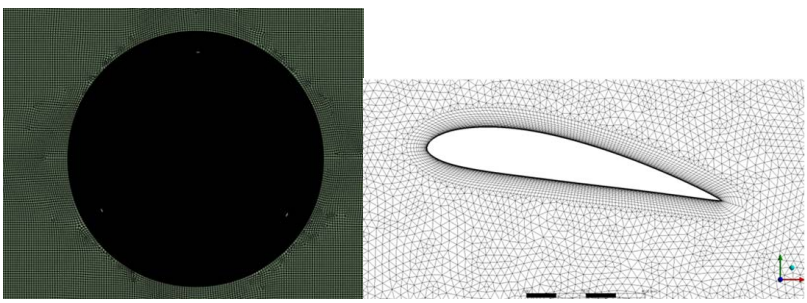

(a) (b)

Figure 4 Mesh. a) General meshing b.) Detail of the meshing of the blade with 20-layer Inflation. Author

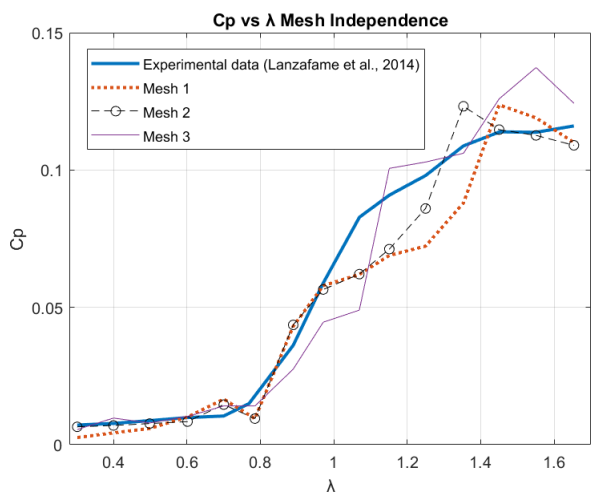

Figure 5 Cp vs λ of the proposed models compared with experimental data [8]

hindering accuracy and convergence. Generally, it is desirable to keep the "skewness" parameter well below 0.95, as values higher than this threshold may lead to convergence difficulties. Regarding the "orthogonal quality" parameter, values close to 1 indicate that the highest quality cells have been achieved, as mentioned in [26]. The mesh can be seen in Figure 4.

As can be seen in Figure 5, as the mesh is refined, different values of Cp are obtained in the figure for each option, and the behavior of the curve also changes. However, between the three meshes in the first values, the difference is not significant, but when the value of λ= 1or higher, the difference increases. Therefore, the chosen was mesh 2 because the results were closer to the experimental data with an average error of 15.10%, while mesh 3 showed an average error of 16.58%. Finally, the mesh 1 obtained an average error of 24.82%.

3.3 CFD analysis of the proposed alternative

In this part, the influence of the height-diameter relation and the chord length was analyzed since, for the same relation, two different chord lengths were analyzed. Two angles of attack (0° and 10°) with two wind velocities (4.5 and $7\ \mathrm{m/s}$), which are the critical and maximum velocities of the Chicamocha Canyon, were analyzed.

In Figures 7 - 12, it can be seen the Cp vs. λ for each alternative, for an AD ratio of 0.25, a maximum Cp of around 0.45 with a velocity of $7m/s$ with an angle of attack of 10° as shown in Figure 8, while the minimum Cp

Table 8 Quality mesh 1. Author

Quality mesh 1				
Parameter	**Minimum Value**	**Maximum Value**	**Average Value**	**Optimal Value**
Aspect Ratio	1.0004	52.338	1.305	To avoid significant changes in general
Skewness	2.07e-7	0.8588	5.51e-2	<0.95
Orthogonal quality	9.68e-2	1	0.96	Values close to 1

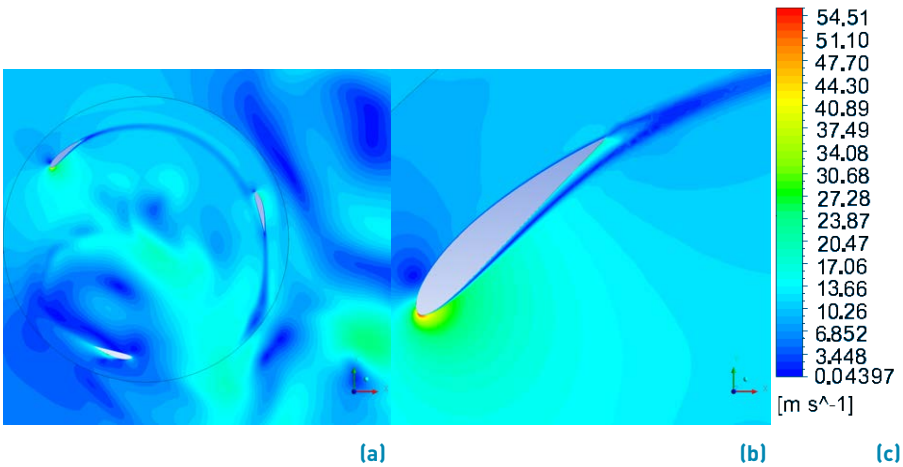

Figure 6 Velocity contour of the mesh independence. a) general contour. b.) blade contour Author

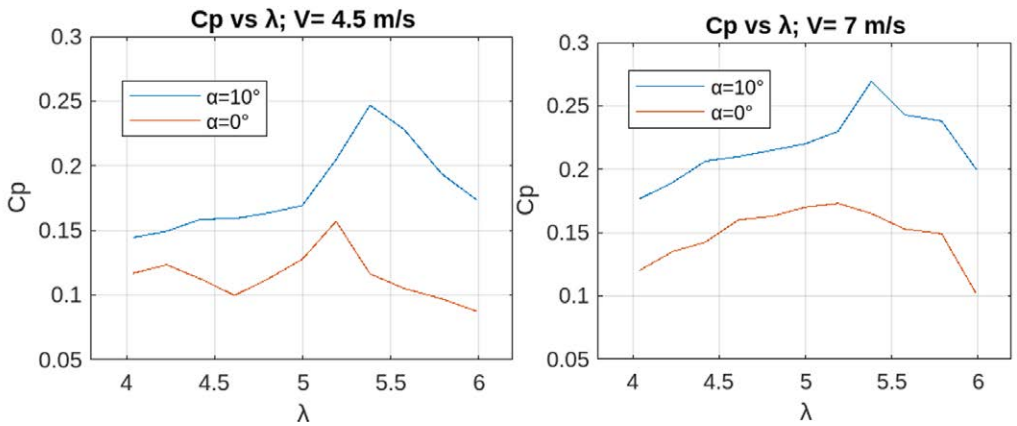

Figure 7 Cp vs λ AD=0.25; c=0.117 m. Author

is around 0.1 at $4.5m/s$ and an angle of attack of 0° as seen in Figure 7.

In Figures 9 and 10, the Cp vs. λ for each AD relation of 0.4 is shown: it can be seen that a maximum Cp of around 0.4 is reached at $7m/s$ with an angle of attack of 10° as can be seen in Figure 10, while the minimum Cp is about 0.1 at a velocity of 4.5 and $7m/s$ with angles of attack of 0° and 10° as seen in Figure 9.

In Figures 11 and 12, Cp vs λ for each AD relation of 1 can be seen, for Cp of around 0.4 is reached at $7m/s$ with an angle of attack of 10° as can be seen in Figure 11, while the minimum Cp is around 0.15 at a velocity of 4.5 and $7m/s$ with angles of attack of 0° and 10° as seen in Figure 12. However, a significant difference is observed in the behavior of the Cp when changing the angle of attack, being a configuration that will depend on much of this value unlike the AD relations of 0.25 and 0.4.

In Figures 13-16, the comparison between each alternative can be seen. The highest Cpprom is presented by option 2 $(AD = 0.25c = 0.173m)$ with a value of 0.31, while the lowest average is by option 3 $(AD = 0.4c = 0.0929m)$

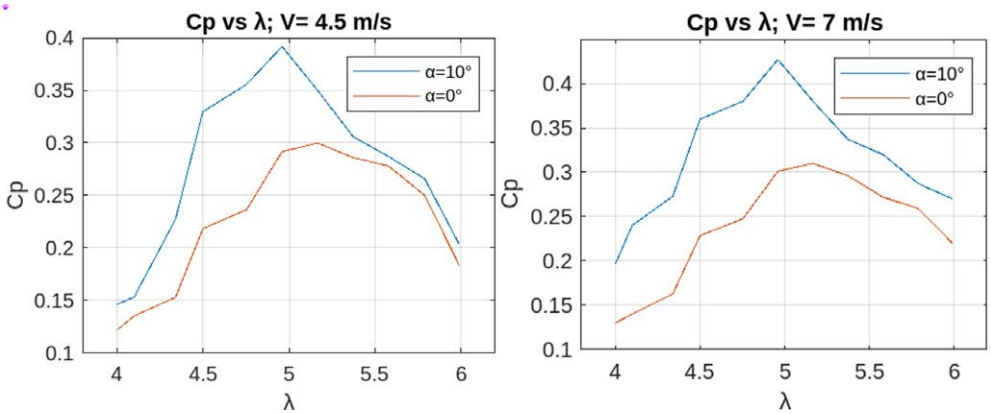

Figure 8 Cp vs λ AD=0.25; c=0.173 m. Author

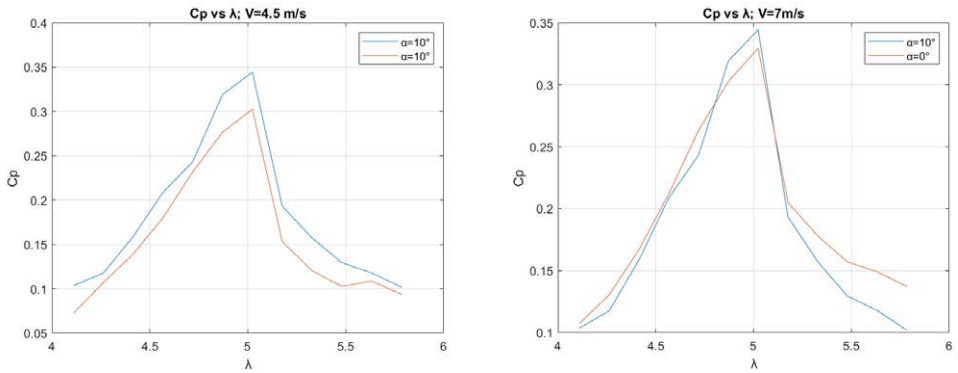

Figure 9 Cp vs λ AD=0.4; c=0.0929 m. Author

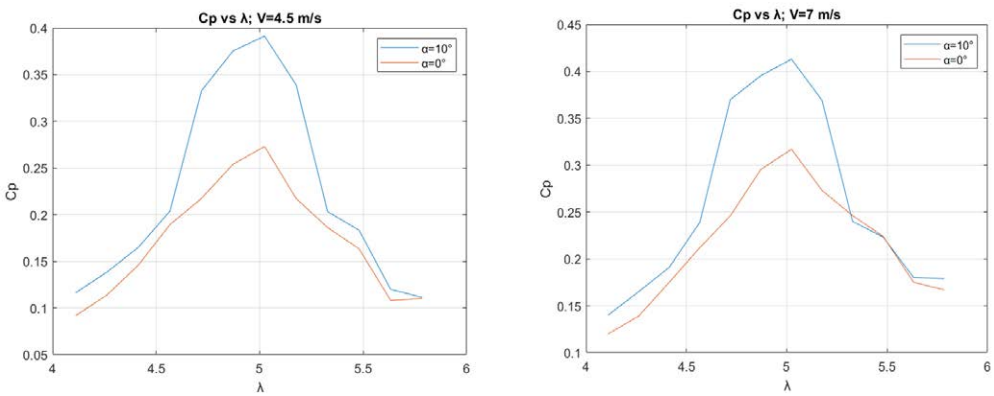

Figure 10 Cp vs λ AD=0.4; c=0.137 m. Author.

with a value of 0.18. It can also be seen that option 2 presents the highest Cp, 0.427 while option 3 obtains the lowest Cp, 0.1018.

In the comparison between the options analyzed, option 2 is the most efficient for the region of interest because at a critical velocity $(4.5m/s)$, it presents better performance than the other options, in addition to increasing the velocity to the maximum found in the Chicamocha Canyon $(7m/s)$ it continues to show good behavior both at 0° and 10°.

Figure 17 represents the velocity contour $(\mathrm{V} = 4.5\ \mathrm{m/s}; \alpha = 0°$ and $alpha = 10°)$ of the better option. In the first part of the figure, the highest velocities occur at the leading and trailing edges of each profile, where a velocity of $34.7m/s$ is reached, while on the intrados and extrados, velocities between $8m/s$ and $27.1m/s$ are reached. As the angle of attack increases, the velocity reached by the aerodynamic profile increases, which is subsequently reflected in the value of the lift and

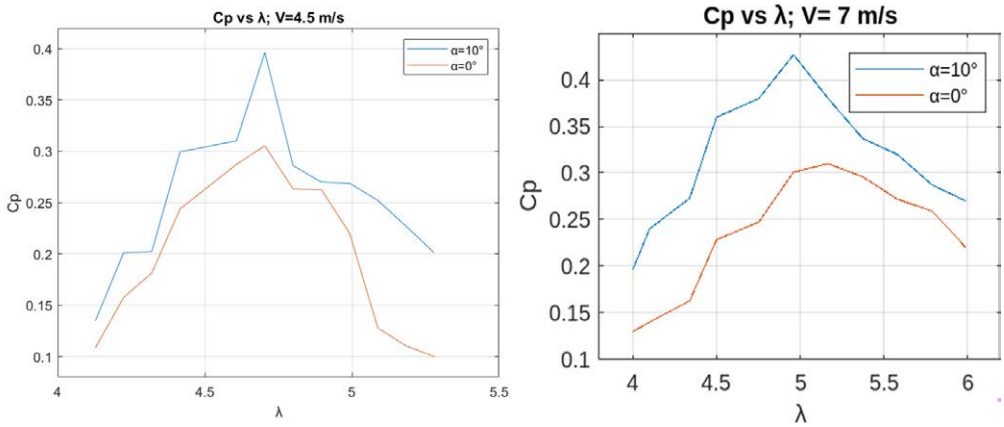

Figure 11 Cp vs λ AD=1; c=0.0587.

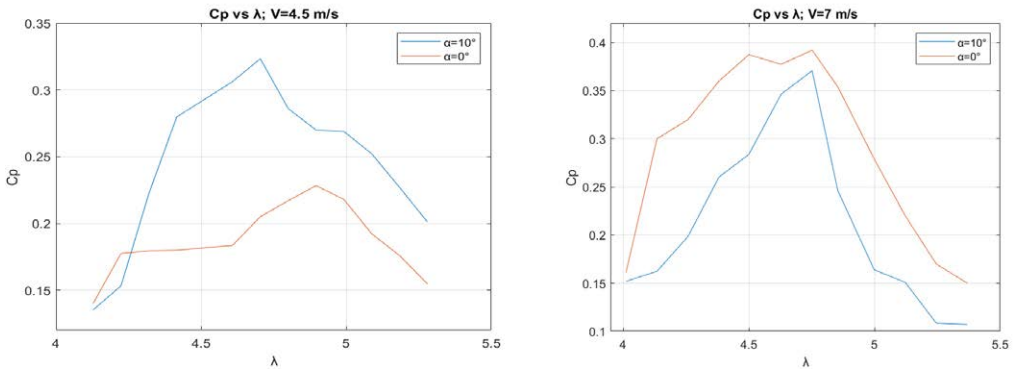

Figure 12 Cp vs λ AD=1; c=0.0864.

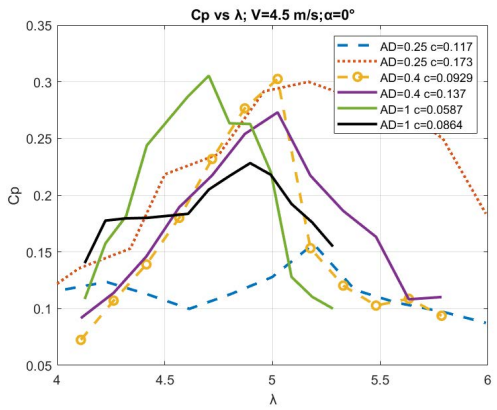

Figure 13 Comparison of performance of alternatives ($\mathrm{V} = 4.5\ \mathrm{m/s} \alpha = 0°$). Author

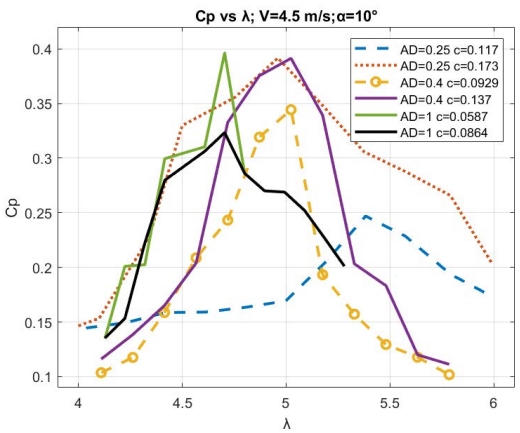

Figure 14 Comparison of performance of alternatives ($\mathrm{V} = 4.5\ \mathrm{m/s} \alpha = 10°$). Author

drag coefficients, whose value is directly related to the performance of the turbine wind (Cp)

In Figure 18, high velocities ranging between 23 and $50m/s$ can occur at the exit of the blade attack at $7m/s$ and 10° in some positions of the blade: this can be generated by the wake-left by the other blades when rotating. When the same speed is analyzed but with an angle of attack of 0°, the same phenomenon does not occur since the free stream velocity is lower, and therefore, the wake does not reach high velocities, which are between 16 and $38m/s$.

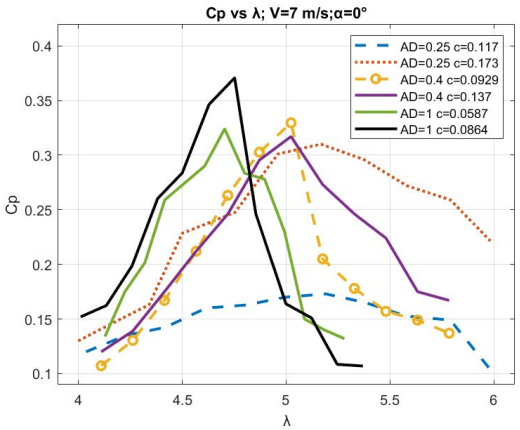

Figure 15 Comparison of performance of alternatives ($V = 7\ m/s \alpha = 0°$). Author

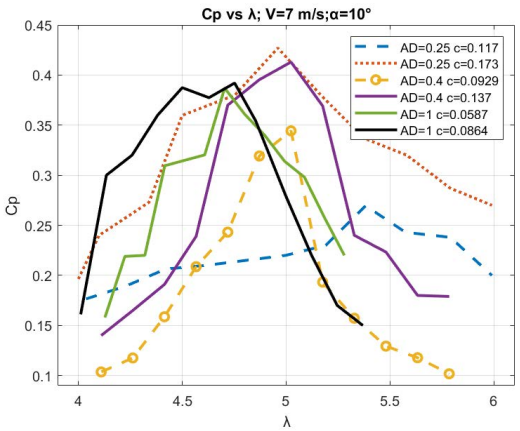

Figure 16 Comparison of performance of alternatives [($V = 7\ m/s \alpha = 10°$)]. Author

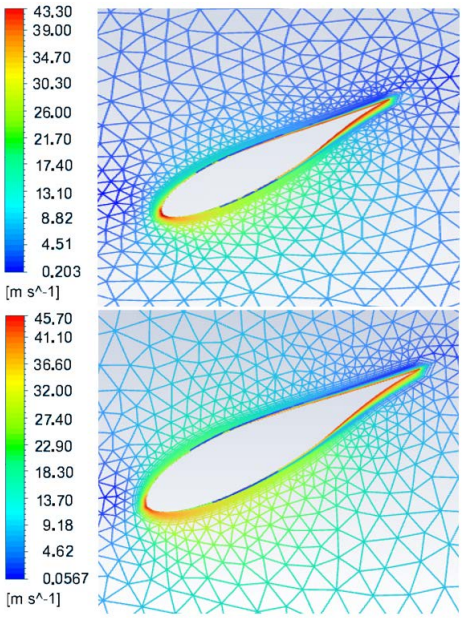

Figure 17 Velocity contour $V = 4.5\ m/s \alpha = 0°$ and $\alpha = 10°$. Author

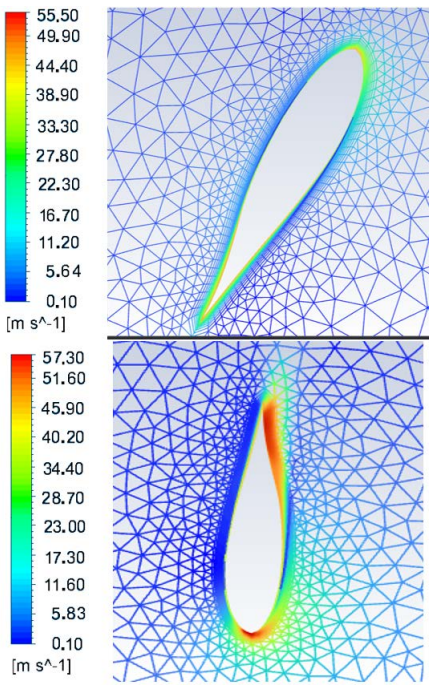

Figure 18 Velocity contour $V = 7\ m/s \alpha = 0°$ and $\alpha = 10°$. Author

4. Conclusions

In summary, this study demonstrates the successful optimization of a three-bladed Darrieus-type vertical axis wind turbine tailored to the unique conditions of the Chicamocha Canyon. The optimization process yielded six promising configurations that meet the specified functional and efficiency requirements and boast impressive validation accuracy, with an error rate consistently under 1%. This lends high credibility to the reliability and accuracy of the optimization algorithm, solidifying its alignment with established literature.

Moreover, the approach of utilizing triangular elements in the rotational zone and rectangular elements in the fixed zone to create a mesh composed of 889,968 elements proved effective. The resulting y+ value of 0.76 within the boundary layer analysis showcased the reliability of the mesh. Despite a minor average error of 15%, the mesh quality values remained comfortably below the recommended thresholds in the literature.

Ultimately, option number two ($AD = 0.25$ and $c = 0.173$) demonstrated superior performance among the considered configurations. It achieved an excellent maximum Power Coefficient Cpprom of 0.31 on average, reaching peak values of up to 0.42. This

level of performance aligns optimally with the specific characteristics of the Chicamocha Canyon, making option number two a highly promising candidate for practical implementation.

5. Declaration of competing interest

We declare that we have no significant competing interests including financial or non-financial, professional, or personal interests interfering with the full and objective presentation of the work described in this manuscript.

6. Acknowledgements

Firstly, to the Vice-Rector for Research and Extension (VIE) of the "Universidad Industrial de Santander" within the 3869-mobility process and to the School of Mechanical Engineering for the financial support received in this research.

7. Funding

This work disclosed receipt of the following financial support for the research, authorship, and/or publication of this article:

8. Author contributions

J.R. Conceived and designed the analysis, performed the analysis, and wrote the paper. J.C Collected the data and wrote the paper. G.G Contributed data analysis tools and advisor.

References

[1] Objetivos de desarrollo sostenible. Organización de las Naciones Unidas. Accessed Apr. 18, 2022. [Online]. Available: https://www.un.org/sustainabledevelopment/es/energy/

[2] L. F. García-Rodríguez and J. L. Chacón-Velasco, "Chicamocha canyon wind energy potential and vawt airfoil selection through cfd modeling," *Revista Facultad de Ingeniería*, vol. 94, Apr. 26, 2019. [Online]. Available: https://doi.org/10.17533/10.17533/udea.redin.20190512

[3] Z. Arifin, D. D. Dwi-Prija-Tjahjana, S. Suyitno, W. E. Juwana, R. A. Rachmanto, C. H. Brillianto-Apribowo, and *et al.*, "Performance of crossflow wind turbines in in-line configuration and opposite rotation direction," *Journal of Advanced Research in Fluid Mechanics and Thermal Sciences*, vol. 81, no. 1, May. 2021. [Online]. Available: https://tinyurl.com/mwdhj2py

[4] I. Paraschivoiu, *Wind Turbine Design: With Emphasis on Darrieus Concept*, 4th ed. Canada: Montreal: Presses Internationales Polytechnique, 2002.

[5] A. Meana-Fernández, I. Solís-Gallego, J. M. Fernández-Oro, K. M. Argüelles-Díaz, and S. Velarde-Suárez, "Parametrical evaluation of the aerodynamic performance of vertical axis wind turbines for the proposal of optimized designs," *Energy*, vol. 147, Mar. 15 2018. [Online]. Available: https://doi.org/10.1016/j.energy.2018.01.062

[6] A. M. Nawfal, A. Sattar, and H. Abdul, "An experimental and numerical investigation on darrieus vertical axis wind turbine types at low wind speed," *International Journal of Mechanical & Mechatronics Engineering IJMME-IJENS*, vol. 19, no. 6, Dec. 2019. [Online]. Available: https://tinyurl.com/ffpbpmzu

[7] K. Hoe-Wong, W. Tong-Chong, S. Chew-Poh, Y. C. Shiah, and C. T. W. N. L. Sukiman and, "3d cfd simulation and parametric study of a flat plate deflector for vertical axis wind turbine," *Renewable Energy*, vol. 129, Dec. 2018. [Online]. Available: https://doi.org/10.1016/j.renene.2018.05.085

[8] J. D. Rosero-Ariza, J. L. Chacón-Velasco, and G. González-Silva, "Análisis comparativo en cfd de seis turbinas vawt para el cañón del chicamocha," *Revista Facultad de Ingeniería*, vol. 111, Apr. 2024. [Online]. Available: https://doi.org/10.17533/udea.redin.20240413

[9] D. D. D. Prija-Tjahjana, Z. Arifin, S. Suyitno, W. E. Juwana, A. Rio-Prabowo, and C. Harsito, "Experimental study of the effect of slotted blades on the savonius wind turbine performance," *Theoretical and Applied Mechanics Letters*, vol. 11, no. 3, Mar. 12, 2021. [Online]. Available: https://doi.org/10.1016/j.taml.2021.100249

[10] S. Brusca, R. Lanzafame, and M. Messina, "Design of a vertical-axis wind turbine: how the aspect ratio affects the turbine's performance," *International Journal of Energy and Environmental Engineering*, vol. 5, Aug. 02, 2014. [Online]. Available: https://doi.org/10.1007/s40095-014-0129-x

[11] M. S. M. Shamsuddin and N. M. Kamaruddin, "Experimental study on the characterization of the self-starting capability of a single and double-stage savonius turbine," *Results in Engineering*, vol. 17, 2022. [Online]. Available: https://doi.org/10.1016/j.rineng.2022.100854

[12] J. He, X. Jin, S. Xie, L. Cao, Y. Wang, Y. Lin, and *et al.*, "Cfd modeling of varying complexity for aerodynamic analysis of h-vertical axis wind turbines," *Renewable Energy*, vol. 145, Jul. 28, 2019. [Online]. Available: https://doi.org/10.1016/j.renene.2019.07.132

[13] D. M. Prabowoputra, A. R. Prabowo, H. Nubli, C. Harsito, Ubaidillah, D. D. Susilo, and *et al.*, "Forecasting effect of blade numbers to cross-flow hydro-type turbine with runner angle 30° using cfd and fda approach," *Mathematical Modelling of Engineering Problems*, vol. 10, no. 2, 2023. [Online]. Available: https://doi.org/10.18280/mmep.100205

[14] B. Zouzou, I. Dobrev, F. Massouh, and R. Dizene, "Experimental and numerical analysis of a novel darrieus rotor with variable pitch mechanism at low tsr," *Energy*, vol. 186, Nov. 1, 2019. [Online]. Available: https://doi.org/10.1016/j.energy.2019.07.162

[15] J. Banega and N. Moreno-Salas, "Diseño aerodinámico de una vawt adecuada a los perfiles de viento de paraguaná mediante cfd," *Revista de la Facultad de Ingeniería*, vol. 31, no. 4, 2016. [Online]. Available: http://saber.ucv.ve/ojs/index.php/rev_fiucv/article/view/15497

[16] H. Day, D. Ingham, L. Ma, and M. Pourkashanian, "Adjoint based optimisation for efficient vawt blade aerodynamics using cfd," *Elsevier*, Oct. 24, 2020. [Online]. Available: https://doi.org/10.1016/j.jweia.2020.104431

[17] J. M. Fernández-Oro, *Técnicas numéricas en ingeniería de fluidos : introducción a la dinámica de fluidos computacional (CFD) por el método de volúmenes finitos*. Reverté, 2012.

[18] R. Lanzafame, S. Mauro, and M. Messina, "2d cfd modeling of h-darrieus wind turbines using a transition turbulence model," *Energy Procedia*, vol. 45, Jan. 29, 2014. [Online]. Available: https://doi.org/10.1016/j.egypro.2014.01.015

[19] F. Balduzzi, A. Bianchini, R. Maleci, G. Ferrara, and L. Ferrari, "Critical issues in the cfd simulation of darrieus wind turbines," *Renewable Energy*, vol. 85, Jun. 16, 2016. [Online]. Available: https://doi.org/10.1016/j.renene.2015.06.048

[20] Y. Li, S. Yang, F. Feng, and K. Tagawa, "A review on numerical simulation based on cfd technology of aerodynamic characteristics of straight-bladed vertical axis wind turbines," *Energy Reports*, vol. 9, Mar. 14, 2023. [Online]. Available: https://doi.org/10.1016/j.egyr.2023.03.082

[21] M. Salman-Siddiqui, M. Hamza-Khalid, R. Zahoor, F. Sarfraz-Butt,

and A. Waheed-Badar, "A numerical investigation to analyze effect of turbulence and ground clearance on the performance of a roof top vertical–axis wind turbine," *Renewable Energy*, vol. 164, Feb. 2021. [Online]. Available: https://doi.org/10.1016/j.renene.2020.10.022

[22] A. J. González-Díaz, L. J. Geovo-Coronado, and Y. E. González-Doria, "Diseño y modelamiento de un aerogenerador vawt darrieus tipo h para la zona costera del departamento de córdoba," *INGENIARE, Universidad Libre-Barranquilla*, vol. 20, 2016. [Online]. Available: https://dialnet.unirioja.es/servlet/articulo?codigo=5980560

[23] A. Posa, "Influence of tip speed ratio on wake features of a vertical axis wind turbine," *Journal of Wind Engineering and Industrial Aerodynamics*, vol. 197, Jan. 03, 2020. [Online]. Available: https://doi.org/10.1016/j.jweia.2019.104076

[24] R. Quiroga and O. A. G.-E. andG. González-Silva, "Effect of temperature on the vapour fraction of heavy crude oil in hydrodynamic cavitation vortex reactor using cfd," *Ciencia en Desarrollo*, vol. 12, no. 2, Jan. 29, 2022. [Online]. Available: https://doi.org/10.19053/01217488.v12.n2.2021.13418

[25] A. S. Alexander and A. Santhanakrishnan, "Mechanisms of power augmentation in two side-by-side vertical axis wind turbines," *Renewable Energy*, vol. 148, no. 2, Oct. 28, 2019. [Online]. Available: https://doi.org/10.1016/j.renene.2019.10.149

[26] A. Inc, "Ansys fluent theory guide," *ANSYS, Inc Canonsburg*, pp. 90 311–2, 2013.